Low-energy tandem mass spectrometry with ion-trap mass spectrometry clearly shows a difference in fragmentation between PtdGlc and PI. Fig. 4 shows a comparison of the on-line MS^2 spectra of 18:0-20:0-PtdGlc (m/z = 893) and 18:0-20:4-PI (m/z = 885). A MS^2 spectrum of PI lacks a peak derived from the neutral loss of inositol–H_2O (m/z = 162) but contains strong peaks formed by the neutral loss of 20:4 and 18:0 acids and subsequent loss of inositol–H_2O. In contrast, the PtdGlc spectrum contains a peak formed by the neutral loss of glucose–H_2O and subsequent loss of 20:0 and 18:0 acids, but the peak intensity of ions derived from fatty acid loss from the molecular ions is very small. These results suggest that the P–O–C bond of phosphoglucose in PtdGlc is more labile than that of phosphoinositol in PI. In PtdGlc, ions arising from the loss of 20:0 are more abundant than those from the loss of 18:0, and similarly those arising from the loss of 20:4 are more abundant in PI. This suggests that both 20:0 and 20:4 tend to

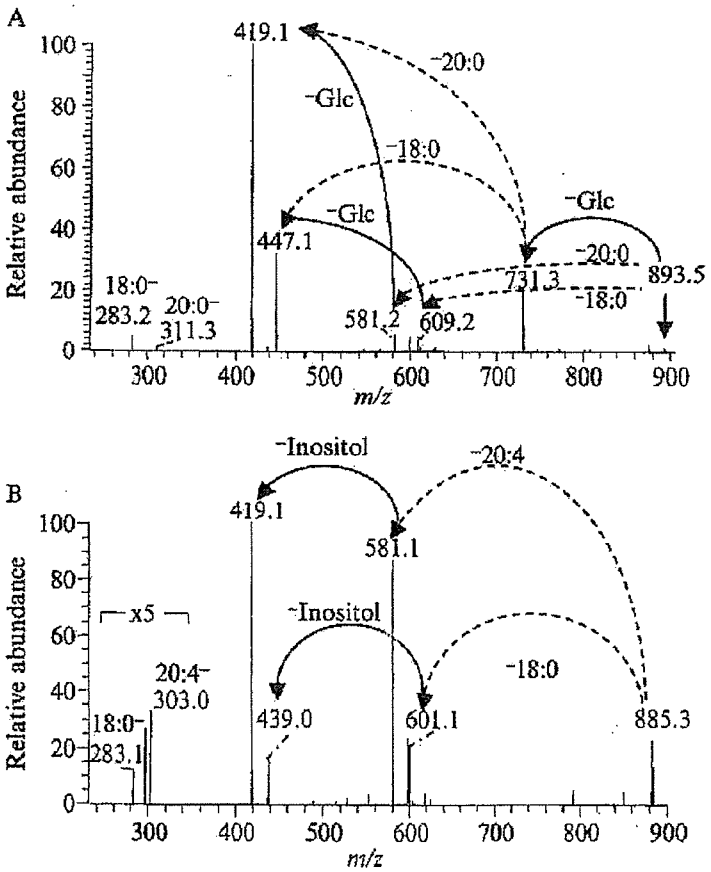

FIG. 4. Comparison of tandem mass spectra of 18:0-20:0-PtdGlc (A) and 18:0-20:4-PI (B). -Glc, loss of glucose–H_2O; -Inositol, loss of inositol–H_2O.

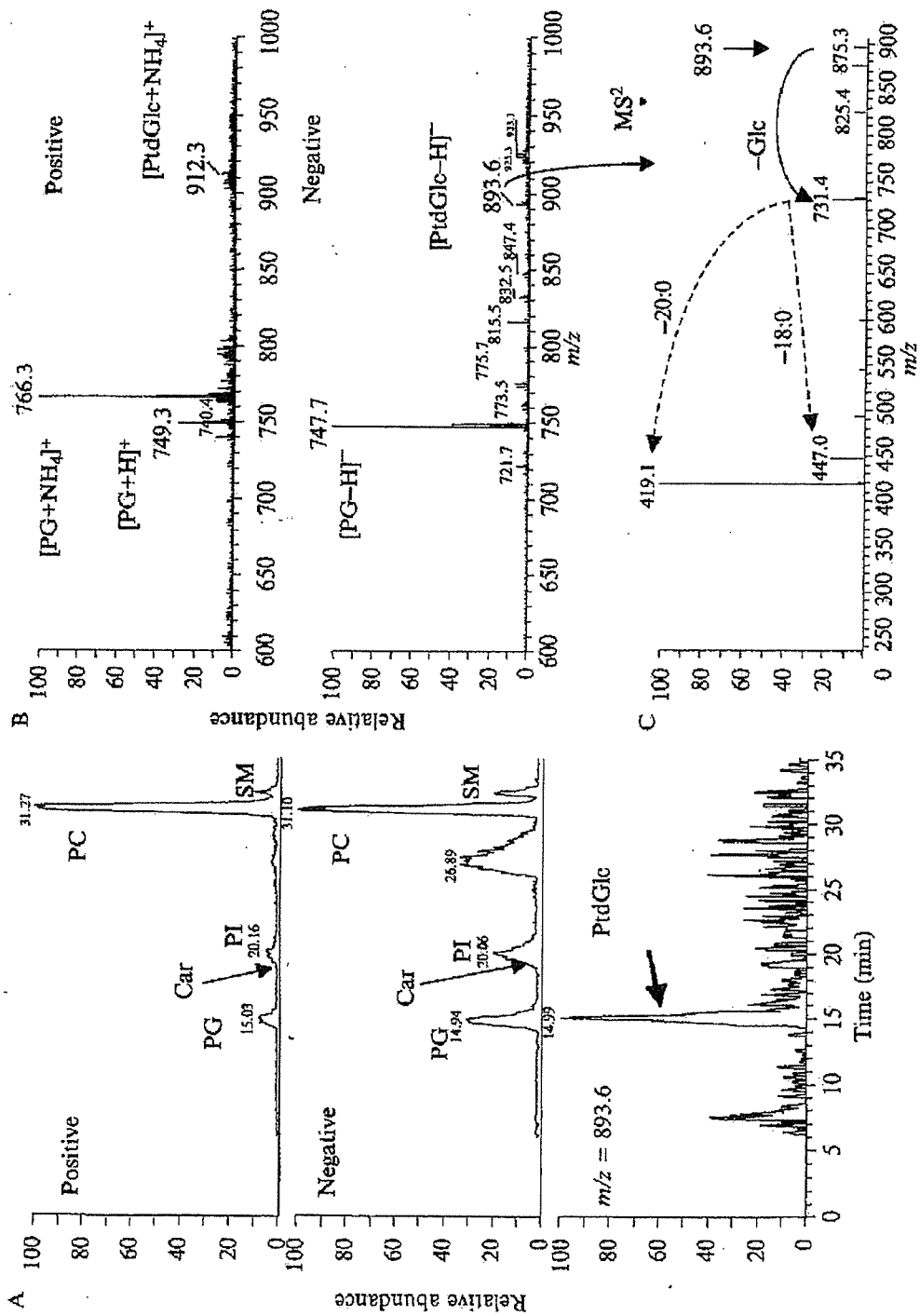

FIG. 5. Analysis of PtdGlc from chick spinal cord. (A) Base-peak chromatograms in the positive and negative ion modes, and ion chromatograms in the negative ion mode at $m/z = 893.6$. Car, cardiolipin. (B) Full-scan MS^2 spectra across a base peak labeled as PG in the positive and negative modes. (C) Tandem mass spectra of $m/z = 893$ ion in B.

be esterified at the *sn*-2 position in PtdGlc and PI, respectively (Larsen *et al.*, 2001). In both spectra, carboxylate anions are less abundant, which is characteristic of collision-induced dissociation in ion-trap MS.

To test the performance of this method, we used lipids extracted from chick spinal cord. The lipids were digested by PIPLC and partially purified by phenylboronate affinity and Q-Sepharose column chromatography. The fraction that exhibited positive reactions with TLC-immunostaining using mAb DIM21 was subjected to HPLC/MS. We found that the DIM21-immunoreactive fraction contained a variety of phospholipids including the major classes of PG, cardiolipin, PI, PC, and sphingomyelin (SM). We still observed an appreciable amount of PI_2 despite extensive digestion with PIPLC. When assessed in negative and positive modes, note that this fraction did contain small but significant $m/z = 893$ and $m/z = 912$ peaks, respectively, in the base peak corresponding to PG ($m/z = 747$), which are suggestive of the presence of 18:0–20:0-PtdGlc. The intensity of these peaks increased in a dose-dependent manner. These peaks were not observed on a blank run. Indeed on-line tandem mass spectrometry of the $m/z = 893$ ions in the negative ion mode confirmed a structure of 18:0-20:0-PtdGlc (Fig. 5C).

References

Brown, D. A., and London, E. (2000). Structure and function of sphingolipid- and cholesterol-rich membrane rafts. *J. Biol. Chem.* **275,** 11721–17224.

Guirland, C., Suzuki, S., Kojima, M., Lu, B., and Zheng, J. Q. (2004). Lipid rafts mediate chemotropic guidance of nerve growth cones. *Neuron* **42,** 51–62.

Herincs, Z., Corset, V., Cahuzac, N., Furne, C., Castellani, V., Hueber, A. O., and Mehlen, P. (2005). DCC association with lipid rafts is required for netrin-1-mediated axon guidance. *J. Cell. Sci.* **118,** 1687–1692.

Ikezawa, H., Yamanegi, M., Taguchi, R., Miyashita, T., and Ohyabu, T. (1976). Studies on phosphatidylinositol phosphodiesterase (phospholipase C type) of *Bacillus cereus* purification, properties and phosphatase-releasing activity. *Biochim. Biophys. Acta* **450,** 154–164.

Ito, M., Tchoua, U., Okamoto, M., and Tojo, H. (2002). Purification and properties of a phospholipase A_2/lipase preferring phosphatidic and lysobisphosphatidic Acids, and monoacylglycerol from rat testis. *J. Biol. Chem.* **277,** 43674–43681.

Kakio, A., Nishimoto, S., Yanagisawa, K., Kozutsumi, Y., and Matsuzaki, K. (2002). Interactions of amyloid beta-protein with various gangliosides in raft-like membranes: Importance of GM1 ganglioside-bound form as an endogenous seed for Alzheimer amyloid. *Biochemistry* **11,** 7385–7390.

Katagiri, Y. U., Ohmi, K., Katagiri, C., Sekino, T., Nakajima, H., Ebata, T., Kiyokawa, N., and Fujimoto, J. (2001). Prominent immunogenicity of monosialosyl galactosylgloboside, carrying a stage-specific embryonic antigen-4 (SSEA-4) epitope in the ACHN human renal tubular cell line-a simple method for producing monoclonal antibodies against detergent-insoluble microdomains/raft. *Glycoconj. J.* **18,** 347–353.

Katagiri, Y-U., Ohmi, K., Tang, W., Takenouchi, H., Taguchi, T., Kiyokawa, N., and Fujimoto, J.. (2002). Raft.1, a monoclonal antibody raised against the raft microdomain, recognizes G-protein beta1 and 2, which assemble near nucleus after shiga toxin binding to human renal cell line. *Lab. Invest.* **82,** 1735–1745.

Larsen, A., Uran, S., Jacobsen, P. B., and Skotland, T. (2001). Collision-induced dissociation of glycerol phospholipids using electrospray ion-trap mass spectrometry. *Rapid Commun. Mass Spectrom.* **15,** 2393–2398.

Mukherjee, A., Arnaud, L., and Cooper, J. A. (2003). Lipid-dependent recruitment of neuronal Src to lipid rafts in the brain. *J. Biol. Chem.* **278,** 40806–40814.

Nagatsuka, Y., Kasama, T., Uzawa, J., Ohashi, Y., Ono, Y., and Hirabayashi, Y. (2001). A new phosphoglycerolipid, "phosphatidylglucose", found in human cord red cells. by multi-reactive monoclonal anti-i cold agglutinin, mAb GL-1/GL-2. *FEBS Lett.* **497,** 141–147.

Nagatsuka, Y., Hara-Yokoyama, M., Kasama, T., Takekoshi, M., Maeda, F., Ihara, S., Fujiwara, S., Obshima, E., Ishii, K., Kobayashi, T., Shimizu, K., and Hirabayashi, Y. (2003). Carbohydrate-dependent signaling from the phosphatidylglucoside based micro-domain induces differentiation of HL60 cells. *Proc. Natl. Acad. Sci. USA* **100,** 7454–7459.

Nagatsuka, Y., Horibata, Y., Yamazaki, Y., Kinoshita, M., Hashikawa, T., Koshino, H., Nakamura, T., and Hirabayashi, Y. (2006). Phosphatidylglucoside with unique fatty acyl chains is present in the murine central nervous system. *Biochemistry* **45,** 8742–8750.

Schaeren-Wiemers, N., Bonnet, A., Erb, M., Erne, B., Bartsch, U., Kern, F., Mantei, N, Sherman, D., and Suter, U. (2004). The raft-associated protein MAL is required for maintenance of proper axon—glia interactions in the central nervous system. *J. Cell. Biol.* **166,** 731–742.

Simons, K., and Ikonen, E. (1997). Functional rafts in cell membranes. *Nature.* **387,** 569–572.

Takagi, S., Tojo, H., Tomita, S., Sano, S., Itami, S., Hara, M., Inoue, S., Horie, K., Kondoh, G., Hosokawa, K., Gonzalez, F. J., and Takeda, J. (2003). Alteration of the 4-sphingenine scaffolds of ceramides in keratinocyte-specific Arnt deficient mice affects skin barrier function. *J. Clin. Invest.* **112,** 1372–1382.

Tojo, H. (2004). Properties of an electrospray emitter coated with material of low surface energy. *J. Chromatogr. A* **1056,** 223–228.

Vinson, M., Rausch, O., Maycox, P-R., Prinjha, R-K., Chapman, D., Morrow, R., Harper, A.J, Dingwall, C., Walsh, F. S., Burbidge, S. A., and Riddell, D. R. (2003). Lipid rafts mediate the interaction between myelin-associated glycoprotein (MAG) on myelin and MAG-receptors on neurons. *Mol. Cell. Neurosci.* **22,** 344–352.

Yamazaki, Y., Nagatsuka, Y., Oshima, E., Suzuki, Y., Hirabayashi, Y., and Hashikawa, T. (2006). Comprehensive analysis of monoclonal antibodies against detergent-insoluble membrane/lipid rafts from HL60 cells. *J. Immunol. Methods* **311,** 106–116.

Yu, W., Zou, K., Gong, J-S., Ko, M., Yanagisawa, K., and Michikawa, M. (2005). Oligomerization of amyloid beta-protein occurs during the isolation of lipid rafts. *J Neurosci. Res.* **80,** 114–119.

Further Reading

Higashi, H., Hirabayashi, Y., Fukui, Y., Naiki, M., Matsumoto, M., Ueda, S., and Kato, S. (1985). Characterization of N-glycolylneuraminic acid-containing gangliosides as tumor-associated Hanganutziu-Deicher antigen in human colon cancer. *Cancer Res.* **45,** 3796–3802.

J. Biochem. **139**, 789–795 (2006)
doi:10.1093/jb/mvj088

Three-Dimensional Structure of Rat-Liver Acyl-CoA Oxidase in Complex with a Fatty Acid: Insights into Substrate-Recognition and Reactivity toward Molecular Oxygen

Keiji Tokuoka[1], Yoshitaka Nakajima[1,*], Ken Hirotsu[1], Ikuko Miyahara[1], Yasuzo Nishina[2], Kiyoshi Shiga[2], Haruhiko Tamaoki[3], Chiaki Setoyama[3], Hiromasa Tojo[4] and Retsu Miura[3,†]

[1]Department of Chemistry, Graduate School of Science, Osaka City University, Sugimoto, Sumiyoshi-ku, Osaka 558-8585; Departments of [2]Molecular Physiology and [3]Molecular Enzymology, Graduate School of Medical Sciences, Kumamoto University, Honjo, Kumamoto 860-8556; and [4]Department of Biochemistry and Molecular Biology, Graduate School of Medicine, Osaka University, Yamadaoka, Suita 565-0871

Received February 5, 2006; accepted March 1, 2006

The three-dimensional structure of rat-liver acyl-CoA oxidase-II (ACO-II) in a complex with a C12-fatty acid was solved by the molecular replacement method based on the uncomplexed ACO-II structure. The crystalline form of the complex was obtained by cocrystallization of ACO-II with dodecanoyl-CoA. The crystalline complex possessed, in the active-site crevice, only the fatty acid moiety that had been formed through hydrolysis of the thioester bond. The overall dimeric structure and the folding pattern of each subunit are essentially superimposable on those of uncomplexed ACO-II. The active site including the flavin ring of FAD, the crevice embracing the fatty acyl moiety, and adjacent amino acid side chains are superimposably conserved with the exception of Glu421, whose carboxylate group is tilted away to accommodate the fatty acid. One of the carboxyl oxygens of the bound fatty acid is hydrogen-bonded to the amide hydrogen of Glu421, the presumed catalytic base, and to the ribityl 2′-hydroxyl group of FAD. This hydrogen-bonding network correlates well with the substrate recognition/activation in acyl-CoA dehydrogenase. The binding mode of C12-fatty acid suggests that the active site does not close upon substrate binding, but remains spacious during the entire catalytic process, the oxygen accessibility in the oxidative half-reaction thereby being maintained.

Key words: acyl-CoA oxidase, complex with a fatty acid, reactivity with oxygen, substrate recognition, three-dimensional structure.

Abbreviations: ACD, acyl-CoA dehydrogenase; ACO, acyl-CoA oxidase; MCAD, medium-chain acyl-CoA dehydrogenase

The fatty acid degradation through β-oxidation in mammals is known to proceed in two different cellular compartments, mitochondria and peroxisomes (see Ref. *1* for a historical overview). The former contain the pathway initiated by acyl-CoA dehydrogenases (ACDs) while the latter foster that initiated by acyl-CoA oxidases (ACOs). An ACO [EC 1.3.3.6] is a flavooxidase with one non-covalently bound FAD per subunit as the prosthetic group and catalyzes dehydrogenation of acyl-CoA yielding *trans*-2-enoyl-CoA in the reductive half-reaction (Scheme 1). ACOs and ACDs belong to the same superfamily (*2*) and cause the same catalytic dehydrogenation of acyl-CoA to the corresponding *trans*-2-enoyl-CoA in the reductive half-reaction. In contrast, they differ completely in the oxidative half-reaction; ACO utilizes molecular oxygen to reoxidize reduced flavin produced in the reductive half-reaction while ACD passes electrons to electron-transferring flavoprotein to regenerate an oxidized flavin (see a recent review Ref. *3* and references cited therein). We have cloned two different isoforms of rat-liver ACO (ACO-I and ACO-II), and separately expressed, purified and characterized them (*4*). We then solved the crystal structure of ACO-II, the first three-dimensional structure of ACO ever solved, and revealed the structural basis for its reactivity toward acyl-CoA as well as toward molecular oxygen (*5*). The three-dimensional structure of a plant ACO was reported very recently and it was shown that its structural features in terms of overall folding as well as active-site architecture closely resemble those of rat ACO-II (*6*).

Although it has been known for quite some time that ACOs and ACDs belong to the same superfamily (*2*) and cause the identical reductive half-reaction, *i.e.*, α-β dehydrogenation of acyl-CoA, the investigation of ACOs on the molecular level has been relatively limited as compared to that of ACDs due primarily to the lack of three-dimensional structures. Moreover, the mechanistic studies (see Ref. *7* for a recent review) on ACDs have mainly been focused on their reductive half-reactions and not much on their oxidative half-reactions. However, the oxidative half-reactions of the ACO-ACD superfamily, particularly

*Present address: Graduate School of Biomedical Sciences, Nagasaki University, 1-14 Bunkyo-machi, Nagasaki 852-8521.

†To whom correspondence should be addressed. Fax: +81-96-373-5066, E-mail: miura@gpo.kumamoto-u.ac.jp

 © 2006 The Japanese Biochemical Society.

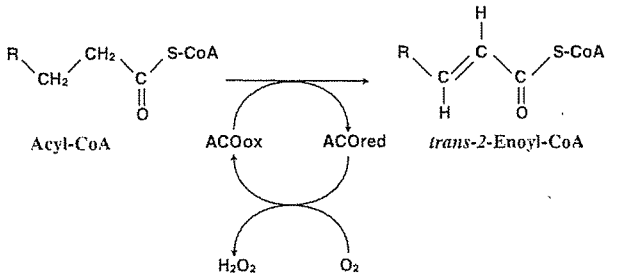

Scheme 1. **Reaction catalyzed by acyl-CoA oxidase (ACO).** ACOox and ACOred stand for the oxidized and reduced forms of ACO, respectively.

their reactivity toward molecular oxygen, are of fundamental importance as to the mechanism of flavoenzymes on the one hand, and as to the physiological roles of ACO and ACD on the other hand. From a mechanistic point of view, we have postulated that the reactivity of reduced flavin toward oxygen is controlled through modulation of the resonance hybridization of an anionic reduced flavin so as to fine-tune the nucleophilicity or electron density of C(4a) of the anionic reduced flavin (*8*). Meanwhile, the reactivity of reduced flavin should be properly controlled in order for a flavoenzyme to play its physiological role; the reaction of ACD with oxygen is strictly suppressed so that electrons from reduced flavin are passed on to the respiratory chain for ATP synthesis. The ATP synthesis would be irrelevantly bypassed were it not for the strict suppression of reaction with oxygen. Thus, the ACO-ACD pair will turn out to be an excellent combination of proteins for studying the mechanism underlying the reaction of the reduced form with molecular oxygen in view of their identical reductive half-reactions but totally different oxidative half-reactions. Both rat ACO-II (*5*) and plant ACO (*6*) are characterized by a spacious active-site pocket and the solvent accessibility favorable for oxygen approach in the oxidative half-reaction. However, these active-site structures have only been demonstrated for the uncomplexed resting state and it remains unknown whether they remain open to oxygen approach when the substrate or product is bound within them. In order to solve these issues we attempted in this study to solve the three-dimensional structure of rat ACO-II in a complex form with a substrate or product. The structure is expected to offer valuable information with respect to substrate recognition/activation in the reductive half-reaction as well as to the reactivity toward molecular oxygen in the oxidative half-reaction.

MATERIALS AND METHODS

Materials—Rat liver ACO-II was expressed in the *Escherichia coli* expression system and purified according to the previously reported procedure (*4*). Dodecanoyl-CoA (lauroyl-CoA) was a product of Sigma and the other chemicals used in this study were from commercial sources and of the highest grade available.

Cocrystallization of ACO-II in the Presence of Dodecanoyl-CoA and Data Collection—The initial crystallization conditions were optimized using Wizard I and II crystal screens (Emerald Biostructures) with 19.0 mg/ml protein and a 100-molar excess of dodecanoyl-CoA in 10 mM Tris-HCl (pH 7.5). Crystals were grown at 293 K by the hanging-drop vapor-diffusion method under oil (*9*). The optimized crystallization conditions involved mixing 2 μl of the protein-ligand mixture with an equivalent volume of a reservoir solution comprising 20% polyethyleneglycol 8000, 2.0 M NaCl and 0.1 M HEPES (pH 7.5). The yellow crystals thus obtained belong to the space group $C222_1$ with one monomer per asymmetric unit, and approximately 48% of the crystal volume is occupied by solvent (*10*). The unliganded enzyme has been reported to be crystallized with the space group $P2_12_12_1$ with one dimer per asymmetric unit (*5*).

Table 1. **Data collection and refinement statistics.**

Data collection	
space group	$C222_1$
lattice parameter (Å)	
a	85.5
b	103.2
c	161.9
temperature (K)	100
wavelength (Å)	1.00
resolution range (Å)	20.0–2.07
no. of reflections	
observation	241,820
unique	43,475 (4,081)[a]
completeness (%)	96.9 (93.6)
R_{merge} [b] (%)	7.6 (28.2)
Refinement	
resolution limit (Å)	41.7–2.07
R_{factor} (%)	19.9 (20.5)
R_{free} (%)	24.1 (25.7)
deviations	
bond lengths (Å)	0.006
bond angles (deg)	1.2
Mean B factors	
main chain atoms (Å^2)	19.8
side chain atoms (Å^2)	22.4
hetero atoms (Å^2)	29.2
waters molecules (Å^2)	28.0

[a]The values in parentheses are for the highest resolution shells. [b]$R_{merge} = \Sigma_{hkl}\Sigma_i|I_{hkl,i} - \langle I_{hkl}\rangle| / \Sigma_{hkl}\Sigma_i I_{hkl,i}$, where I = observed intensity and $\langle I\rangle$ = average intensity for multiple measurements.

The X-ray diffraction data set was collected to 2.07-Å resolution at 100 K using the wavelength of 1.00 Å on NW-12A stations equipped with an ADSC Quantum 4R CCD detector system at the Photon Factory, KEK (Tsukuba, Japan). A cryoprotectant solution of 13% glycerol in the reservoir buffer was used for flash-freezing of the crystals in liquid nitrogen. The data set was processed and scaled using program HKL2000 (*11*) (Table 1).

Structure Determination and Refinement—The structure of the ACO-II complex was determined with program AmoRe (*12*), using the previously determined structure of the unliganded ACO-II (*5*, PDB ID: 1IS2) monomer as a search model. The modeling of the polypeptide chain was performed using program O (*13*). The structure was refined by simulated annealing and energy minimization with program CNS (*14*). When the R_{factor} value decreased to below 30%, the difference Fourier map around the active site exhibited a residual electron density corresponding to

the acyl moiety of dodecanoyl-CoA, but no clear electron density for the CoA moiety was observed. As the result of ligand extraction and mass-spectroscopic analysis, 3-hydroxydodecanoate, the major component of the bound fatty acid, was assigned to the peak in a simulated annealing $2Fo - Fc$ map. Water molecules were picked up from the $2Fo - Fc$ map on the basis of the peak height (1.0 σ) and distance criteria (4.0 Å from protein and solvent). The water molecules with thermal factors above 40 $Å^3$ were removed from the list. Further model building and refinement cycles resulted in an R_{factor} of 20.1% and an R_{free} of 24.3%, calculated for 42,480 reflections (Table 1). During the last step of the refinement, unambiguous water molecules were added including those with temperature factors higher than 40 $Å^3$. The occupancy factor of 3-hydroxydodenanoate was determined to be 0.87. The model lacks 32 residues (270–280, 355–364, 459–474) due to uninterpretable electron density. The lack of two loop regions (270–280, 459–474) is also shared by unliganded ACO-II (*5*). Alanine models were applied to 6 residues (113, 114, 352, 353, 354, 365), because no interpretable electron density was observed for their side chains. The model was of good quality with almost all the residues falling in the most favorable (93.5%) and allowed regions (6.1%) of the Ramachandran plot, when the stereochemistry was assessed with PROCHECK (*15*). Trp176 was assigned in the disallowed region, as it was for the unliganded enzyme (*5*). This may be related with the orientation of the side chain; the indole ring of Trp176 is in a stacking orientation as to the flavin ring, covering the *si*-face of flavin, while the *re*-face is occupied by the fatty acid (see "RESULTS AND DISCUSSION").

Extraction of Fatty Acids from the Crystal Preparation and Mass Spectroscopic Analysis—After crystals had been allowed to grow in the cocrystallization mixture, the preparation mixture was diluted 24 times with 0.4 N HCl containing 1% KCl to decrease the protein concentration and viscosity. Fatty acids were extracted into the upper phase by the two-phase partition method of Dole and Meinertz (*16*). The upper phase was transferred to a new glass tube and then evaporated under a nitrogen gas flow. The extracted fatty acids were dissolved in methanol containing 10 mM ammonium formate, and then directly infused into the electrospray ionization (ESI) source in a Mariner ESI/time-of-flight mass spectrometer at the flow rate of 5 µl/min. An ESI voltage of 3 kV and a nozzle potential of 80 V were applied.

RESULTS AND DISCUSSION

Structure of ACO-II in a Complex with a Ligand—We attempted to obtain the crystalline form of the ACO-II-ligand complex by soaking substrates and substrate analogs in crystalline ACO-II. However, all the soaking experiments were unsuccessful due to cracks developing in the crystals. We subsequently cocrystallized ACO-II in the presence of substrate dodecanoyl-CoA (lauroyl-CoA) and obtained crystals of ACO-II with a bound ligand. The overall dimeric structure of cocrystallized ACO-II is shown in Fig. 1. As will be shown later, the ligand bound in the active site is drawn as 3-hydroxydodecanoate, the predominant component of the bound ligand. The two subunits are correlated with each other through a crystallographic two-fold axis. The overall folding pattern of the dimeric complex is practically superimposable on that of uncomplexed ACO-II (*5*). This is better envisaged when the equivalenced Cα atoms of the subunit structures of complexed ACO-II are superposed on those of uncomplexed ACO-II (Fig. 2). These observations suggest strongly that the protein conformation does not change upon ligand binding, which is contrary to our previous expectation that the active site might close when the substrate binds to it (*5*). Namely, the active site remains spacious irrespective of whether the enzyme is in the resting state with a vacant active site or in the acting state with a substrate or product bound in the active site and, therefore, oxygen can freely gain access to the reduced form of flavin during the oxidative half-reaction.

Active Site and Ligand-Binding Mode—Figure 3 shows superpositioning of the active sites for the uncomplexed and complexed states, the latter embracing the fatty acid moiety derived from the substrate dodecanoyl-CoA. As will be shown in the subsequent section, the fatty acid species extracted from the cocrystallization preparation is a mixture of dodecenoate and hydroxydodecanoate, the latter predominating over the former. Though the electron density for the ligand should reflect the weighted average of the two components, the electron density in Fig. 4 is fitted to the predominant component, 3-hydroxydodecanoate (see the subsequent section for structural assignment of the ligand). It is noteworthy that only electron density for the fatty acid moiety on the *re*-face of the flavin ring, *i.e.*, none corresponding to the CoA segment, was observed in the substrate-binding pocket. Although not shown in Fig. 4, the indole ring of

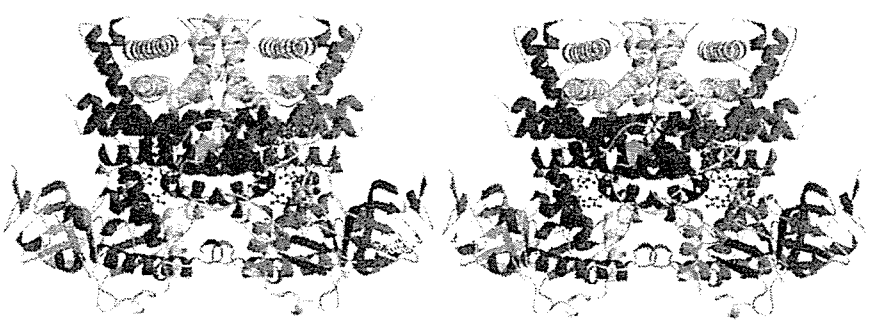

Fig. 1. **Stereoview of the overall dimeric structure of ACO-II cocrystallized with dodecanoyl-CoA.** Note that the bound ligand is 3-hydroxydodecanoate drawn as a CPK model. The coenzyme FAD is drawn as a ball-and-stick model.

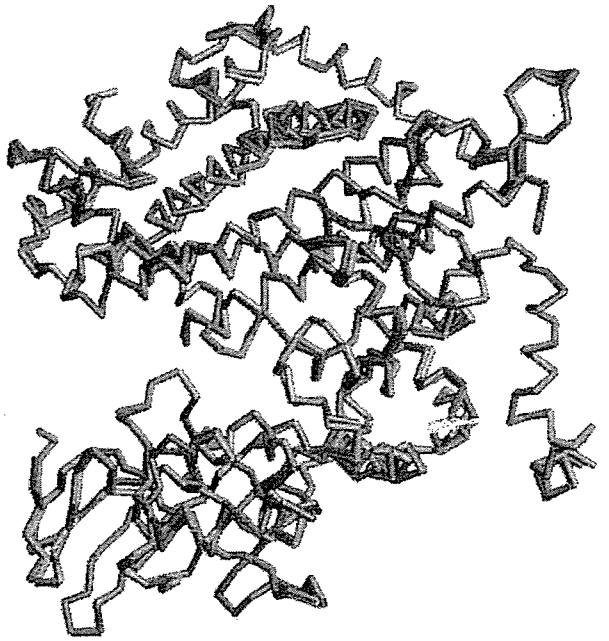

Fig. 2. **Superpositioning of Cα-tracings of complexed (green) and uncomplexed (red) ACO-II.**

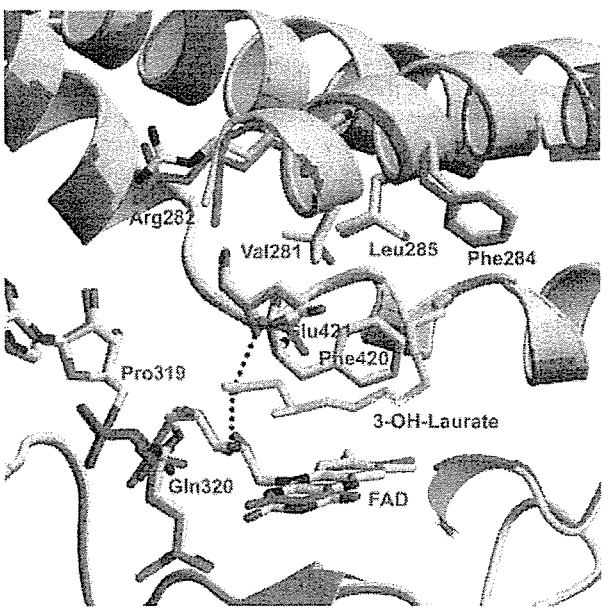

Fig. 3. **Superpositioning of the active-site structures of complexed (grey with oxygen and nitrogen in red and blue, respectively) and uncomplexed (green) ACO-II.** 3-Hydroxydodecanoate is drawn in yellow. Blue dotted lines represent the hydrogen bonding network between the carboxyl oxygen of the bound fatty acid with the backbone amide group of Glu421 and the ribityl-2′-hydroxyl group of FAD.

Trp176 covers the *si*-face, as it does in the unliganded structure (*5*). The hydrocarbon chain of the fatty acid extends along the acyl chain-binding crevice and its length matches that of the C-12 fatty acid included in the substrate dodecanoyl-CoA that was cocrystallized with ACO-II. The side chain of Glu421, the postulated catalytic base that abstracts the α-proton of acyl-CoA (*5*), has changed its orientation in the complexed state, pointing away from the flavin ring to accommodate the fatty acyl moiety. Note the proximity, the interatomic distance being 3.1 Å, of the α-carbon of the bound fatty acid and one of the carboxyl oxygens of Glu421 (dotted line in Figs. 4 and 5), the presumed catalytic base for abstraction of the α-proton of substrate. The mutual alignment of the fatty acid, Glu421 carboxylate and FAD, with the interatomic distances, is illustrated in Fig. 5. The positioning of the carboxyl oxygen relative to the fatty acid α-position is indicative that the Glu421 carboxylate is the catalytic base for abstraction of the substrate α-proton, which is activated by the hydrogen-bonding network at the thioester carbonyl, as discussed below (Scheme 2).

One of the carboxyl oxygens of the C-12 fatty acid is hydrogen-bonded to the ribityl-2′-hydroxyl group of FAD and to the backbone amide hydrogen of Glu421, the catalytic base (Fig. 3, dotted lines, and Fig. 5, thick dashed lines). The interatomic distances corresponding to these hydrogen bonds are 2.5 and 2.9 Å, respectively. This hydrogen-bonding network is reminiscent of that for the recognition and activation of substrate acyl-CoA in medium-chain acyl-CoA dehydrogenase (MCAD) (*17*), the most extensively investigated member of the ACD family; the carbonyl oxygen of the substrate thioester forms a hydrogen bond with the ribityl-2′-hydroxyl group of FAD and with the main-chain amide of Glu376, the catalytic base, and these hydrogen bonds cooperatively play a critical role in lowering the pK_a of the substrate α-proton, thereby activating the substrate for deprotonation by the catalytic base. An identical hydrogen-bonding network is found at the thioester carbonyl oxygen of 3-thiaoctanoyl-CoA in a complex with MCAD (*18*). This MCAD-3-thiaoctanoyl-CoA complex has been regarded as a transition-state analog for the reductive half-reaction of MCAD (*18*, *19*). Although the carboxyl group of the fatty acid bound may differ from the thioester moiety of acyl-CoA in its reactivity and structure, the similarity of the hydrogen-bonding network (Figs. 3 and 5) to that of MCAD and the proximity of the Glu421 carboxylate to the fatty acid α-carbon (Figs. 4 and 5) strongly suggest that ACO-II and MCAD share identical machinery for substrate activation/recognition in their reductive half-reactions (Scheme 2). Another point of fundamental importance with respect to catalysis is that the active site does not close upon substrate/product-binding. This implies that the active-site crevice surrounding the flavin ring maintains its ample space regardless of whether the enzyme is in the uncomplexed resting state or in the acting state engaged in the catalytic event with a substrate or product or the intermediate bound therein. Hence, the approach of molecular oxygen to reduced flavin in the oxidative half-reaction is without significant impediment and the oxidative half-reaction with oxygen is structurally favored.

Identification of the Bound Ligand and the Mechanism of Formation—The structure of ACO-II cocrystallized with dodecanoyl-CoA has revealed the presence of a fatty acid species bound within the active-site crevice, as described above. During the cocrystallization experiments and treatments thereafter, we found out that once cocrystallization

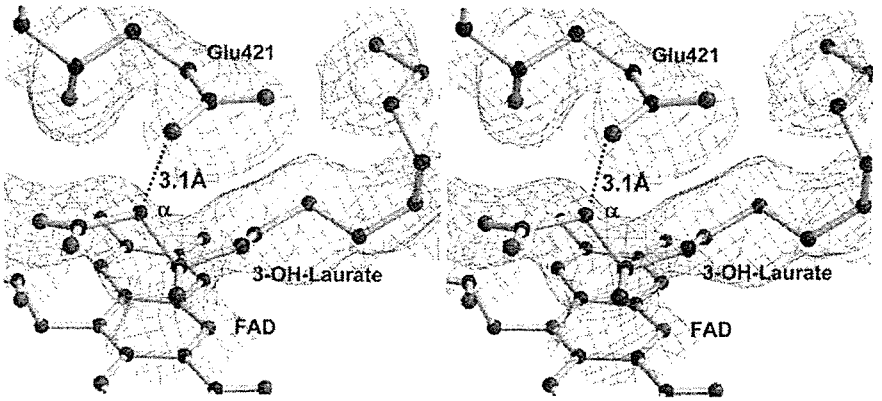

Fig. 4. **Stereo drawing of the 2*Fo*–*Fc* electron density map for bound 3-hydroxydodecanoate and Glu421 contoured at 0.5 σ.**

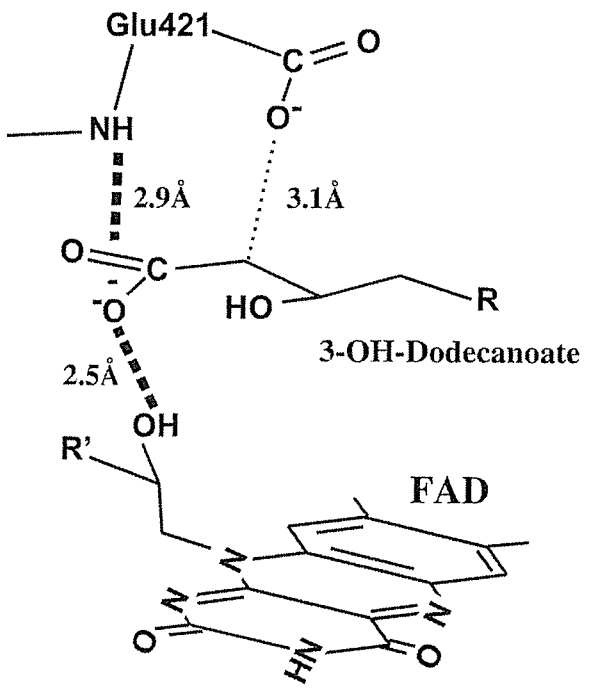

Fig. 5. **Hydrogen-bonding network (thick dashed lines) at the carboxyl oxygen of fatty acid.** The dotted line shows the interatomic distance of 3.5 Å between the α-carbon of the bound fatty acid and the carboxyl oxygen of Glu421 in uncomplexed ACO-II (see text for details).

was completed further added dodecanoyl-CoA did not exchange with the bound fatty acid, *i.e.*, the crystals showed electron density only for the fatty acid, *i.e.*, none for the CoA moiety (results not shown). Furthermore, the addition of dodecanoate to crystalline unliganded ACO-II did not result in the formation of a crystalline ACO-II-fatty acid complex. These observations and the reaction mechanism described below support the idea that the fatty acid species bound in the active site of the crystalline ACO-II are formed during catalysis and in equilibrium with those in the mother liquor. However, the precise structure of the bound ligand remained ambiguous at this point, since the electron-density map was not sufficient to distinguish whether the bound fatty acid is saturated or unsaturated, or includes other minor modifications. So we extracted the fatty acid species from hanging drops containing crystals grown in the presence of excess dodecanoyl-CoA (see "MATERIALS AND METHODS"). The extracts were then subjected to mass spectral analyses. The results shown in Fig. 6 clearly indicate only two mass spectral species at m/z 197.1 and 215.1. The former corresponds to dodecenoate, *i.e.*, mono-unsaturated C12 fatty acid (C12:1), while the latter, the predominant species, can be assigned as hydroxylated dodecanoate. Furthermore, the peak at m/z 199.1 corresponding to dodecanoate (C12:0), the saturated fatty acid, is buried, if present, within the second isotope peak of C12:1. This indicates that non-enzymatic hydrolysis of dodecanoyl-CoA or its inefficient hydrolysis catalyzed at a site other than the active site of crystalline ACO-II hardly occurred, further suggesting mechanism-based formation of the fatty acids within the active site. Dehydration by electric energy may convert hydroxydodecanoate to dodecenoate (C12:1) to a lower extent, which somewhat decreases the peak height ratio of hydroxylated to monoene acids.

So the peak at m/z 197.1 in Fig. 6 includes a very minor contribution from mass spectrometry-driven dehydration of hydroxydodecanoate. The appearance of the peak at m/z 215.1 corresponding to hydroxylated dodecanoate in addition to that for dodecenoate was unexpected at the first sight. However, it can be rationalized on the basis of the active-site structure as well as of the substrate-activating machinery. The presence of two fatty acid species, dodecenoate and hydroxydodecanoate, bound within the active-site crevice can be rationalized by dehydrogenation of dodecanoyl-CoA, as the result of normal catalysis, accompanied by the reaction of water with the dehydrogenated product, dodecenoyl-CoA (Scheme 2). During the cocrystallization of ACO-II in the presence of dodecanoyl-CoA, the enzyme in solution turns over, which produces *trans*-2-dodecenoyl-CoA. But once crystals start to form, dodecanoyl-CoA bound to the active site in a favorable orientation for catalysis undergoes rapid dehydrogenation, which converts the substrate to *trans*-2-dodecenoyl-CoA. However, the product-release from the crystalline enzyme is not as fast as in solution, and the product is held for some time within the active site, the hydrogen-bonding

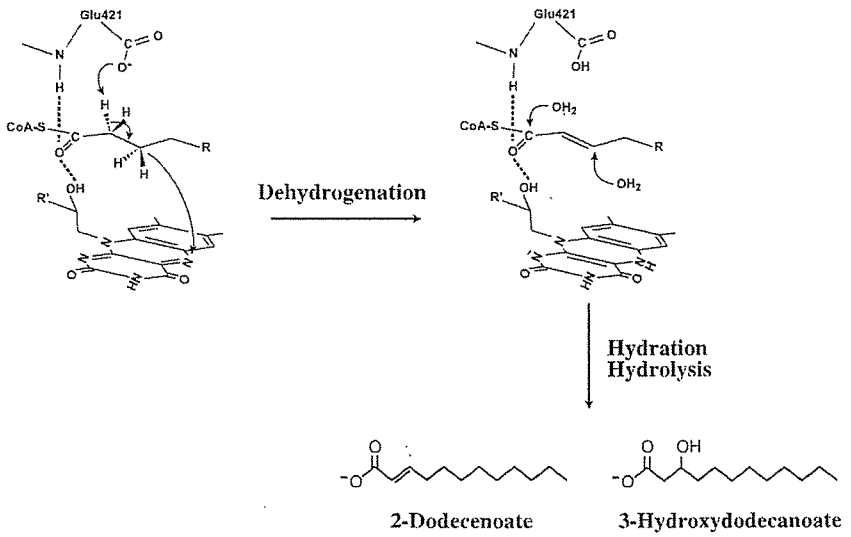

Scheme 2. **The mechanism underlying the reaction of dodecanoyl-CoA during crystal growth and within crystals.**

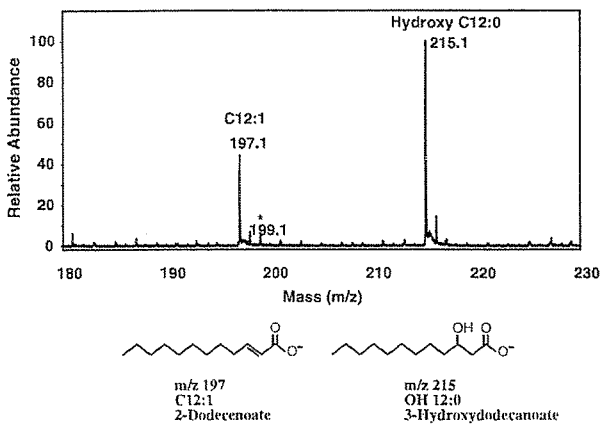

Fig. 6. **Mass spectrogram of the fatty acid species extracted from the crystal preparation of ACO-II in the presence of substrate dodecanoyl-CoA.**

network between thioester carbonyl oxygen and the ribityl-2′-hydroxyl as well as the back-bone amide of Glu421 being retained. This hydrogen-bonding network in turn activates the carbonyl carbon and/or the C(3)-methine carbon of bound dodecenoyl-CoA. As the active-site crevice remains ample during catalysis, water can gain free access to either the carbonyl carbon or C(3)-methine carbon of dodecenoyl-CoA in a Michael-addition type reaction. If water initially attacks the activated carbonyl carbon, thioester is hydrolyzed, which produces dodecenoate, which remains attached to the hydrophobic environment. On the other hand, if water first attacks the C(3)-methine carbon followed by the carbonyl carbon, 3-hydroxydodecanoate forms as the result of Michael addition of water and stays in the hydrophobic pocket. *trans*-2-Dodecenoyl-CoA, which has accumulated during turnover in solution before ACO-II crystallizes, may also penetrate into the active site and will have the same fate as that of the product formed *in situ*, 2-dodecenoate and 3-hydroxydodecanoate eventually being generated. We think that this scenario is a crystallographic artifact primarily due to slow product-release in the crystalline state. Under physiological conditions, however, product-release in solution is much faster and the enzyme turns over preferentially before water attacks the bound product. It should be strongly emphasized, though, that the proposed mechanism for the crystallographic artifact shown in Scheme 2 reflects the inherent modus operandi of ACO-II; the ample active site that allows access of oxygen also allows access of water molecules, and the hydrogen-bonding network at the thioester carbonyl of the substrate activates the substrate for dehydrogenation, but it also activates the product for nucleophilic attack of water in the crystalline state of ACO-II.

We have solved the first structure of ACO in a complex form with a ligand. Although the bound ligand only represents the fatty acid moiety of the substrate or product, the structure has suggested a fundamental mechanism for substrate recognition and activation. Whether or not the conformation and the orientation of the fatty acid bound to the active site accurately reflect the substrate/product-binding mode will be revealed by subsequent study. To answer this question as well as to better understand the substrate activation and the catalytic event at the atomic level, we are attempting to form crystalline ACO in a complex with substrate analogs with a CoA moiety that is not easily hydrolyzed when bound to the active site.

The coordinates for ACO-II in a complex with 3-hydroxydodecanoate have been deposited in the RSCB Protein Data Bank under entry number 2DDH.

This work is supported in part by the National Project on Protein Structural and Functional Analyses.

REFERENCES

1. Ghisla, S. (2004) β-Oxidation of fatty acids. A century of discovery. *Eur. J. Biochem.* **271**, 459–461

2. Matsubara, Y., Indo, Y., Naito, E., Ozasa, H., Glassberg, R., Vockley, J., Ikeda, Y., Kraus, J., and Tanaka, K. (1989) Molecular cloning and nucleotide sequence of cDNAs encoding the precursors of rat long chain acyl-coenzyme A, short chain acyl-coenzyme A, and isovaleryl-coenzyme A dehydrogenases. Sequence homology of four enzymes of the acyl-CoA dehydrogenase family. *J. Biol. Chem.* **264**, 16321–16331
3. Kim, J.-J.P. and Miura, R. (2004) Acyl-CoA dehydrogenases and acyl-CoA oxidases. Structural basis for mechanistic similarities and differences. *Eur. J. Biochem.* **271**, 483–493
4. Setoyama, C., Tamaoki, H., Nishina, Y., Shiga, K., and Miura, R. (1995) Functional expression of two forms of rat acyl-CoA oxidase and their substrate specificities. *Biochem. Biophys. Res. Commun.* **217**, 482–487
5. Nakajima, Y., Miyahara, I., Hirotsu, K., Nishina, Y., Shiga, K., Setoyama, C., Tamaoki, H., and Miura, R. (2002) Three-dimensional structure of the flavoenzyme acyl-CoA oxidase-II from rat liver, the peroxisomal counterpart of mitochondrial acyl-CoA dehydrogenase. *J. Biochem.* **131**, 365–374
6. Pedersen, L. and Henriksen, A. (2005) Acyl-CoA oxidase 1 from *Arabidopsis thaliana*. Structure of a key enzyme in plant lipid metabolism. *J. Mol. Biol.* 345, 487–500
7. Ghisla, S. and Thorpe, C. (2004) Acyl-CoA dehydrogenases. A mechanistic overview. *Eur. J. Biochem.* **271**, 494–508
8. Mizutani, H., Miyahara, I., Hirotsu, K., Nishina, Y., Shiga, K., Setoyama, C., and Miura, R. (2000) Three-dimensional structure of the purple intermediate of porcine kidney D-amino acid oxidase. Optimization of the oxidative half-reaction through alignment of the product with reduced flavin. *J. Biochem.* **128**, 73–81
9. Chayen, N.E. (1997) A novel technique to control the rate of vapour diffusion, giving larger protein crystals, *J. Appl. Cryst.* **30**, 198–202
10. Matthews, B.W. (1968) Solvent content of protein crystals. *J. Mol. Biol.* **33**, 491–497.
11. Otwinowski, Z. and Minor, W. (1997) Processing of X-ray diffraction data collected in oscillation mode. In *Methods in Enzymology* (Carter, C.W., Jr. and Sweet, R.M., eds.) Vol. 276 Part A, pp. 307-326, Academic Press, New York
12. Navaza, J. (1994) *AMoRe*: an automated package for molecular replacement. *Acta Cryst.* **A50**, 157–163
13. Jones, T.A., Zou, J.Y., Cowan, S.W., and Kjeldgaard, M. (1991). Improved methods for building protein models in electron density maps and the location of errors in these models. *Acta Cryst.* **A47**, 110–119
14. Brunger, A.T., Adams, P.D, Clore, G.M., DeLano, W.L., Gros, P., Grosse-Kunstleve, R.W., Jiang, J-S., Kuszewski, J., Nilges, M., Pannu, N.S., Read, R.J., Rice, L.M., Simonson, T., and Warren, G.L. (1998) Crystallography & NMR system: A new software suite for macromolecular structure determination. *Acta Cryst.* **D54**, 905–921
15. Laskowski, R. A., MacArthur, M.W., Moss, D.S., and Thornton, J.M. (1993) *PROCHECK*: a program to check the stereochemical quality of protein structures. *J. Appl. Cryst.* **26**, 283–291
16. Dole, V.P. and Meinertz, H. (1960) Microdetermination of long-chain fatty acids in plasma and tissues. *J. Biol. Chem.* **235**, 2595–2599
17. Kim, J.-J.P., Wang, M., and Paschke, R. (1993) Crystal structures of medium-chain acyl-CoA dehydrogenase from pig liver mitochondria with and without substrate. *Proc. Natl. Acad. Sci. USA* **90**, 7523–7527
18. Satoh, A., Nakajima, Y., Miyahara, I., Hirotsu, K., Tanaka, T., Nishina, Y., Shiga, K., Tamaoki, H., Setoyama, C., and Miura, R. (2003) Structure of the transition state analog of medium-chain acyl-CoA dehydrogenase. Crystallographic and molecular orbital studies on the charge-transfer complex of medium-chain acyl-CoA dehydrogenase with 3-thiaoctanoyl-CoA. *J. Biochem.* **143**, 297–304
19. Lau, S.M., Brantley, R.K., and Thorpe, C. (1988) The reductive half-reaction in acyl-CoA dehydrogenase from pig kidney: studies with thiaoctanoyl-CoA and oxaoctanoyl-CoA analogues. *Biochemistry* **27**, 5089–5095

第９章.

9.2 リピドミクス

大阪大学大学院医学系研究科　東城　博雅

(1) 脂質代謝とリピドミクス

生体機能は、遺伝子にコードされる情報に基づいて発現する蛋白質(酵素)と酵素により生合成・代謝される各種の低分子代謝中間体の働きにより円滑に営まれる。したがって、生体分子間相互作用の複雑なネットワークを解きほぐし生体機能の分子機構を解明するためには、蛋白質と代謝中間体の総覧的分析を相補的に行うことが重要である。主に代謝中間体の構造情報と濃度変動を高感度に検出できる質量分析(MS)法の進歩により、種々の生体反応における代謝中間体の動態を一斉分析することが可能になってきた。これを生体機能解析、医学・創薬・健康保健分野におけるバイオマーカーの探索、食品・栄養・油脂・化粧品・海洋生物・環境などの研究・開発に応用する学問をメタボロミクスと総称する。代謝中間体のうち以下のような特長を持つ水に不溶な脂質を対象とする場合、特別にリピドミクスと呼ぶ。

脂質それ自身は低分子化合物であるが、水溶液中では自己会合して細胞形成に必須の生体膜二重層構造を形成し、受容体などの情報伝達機構のプラットフォームを提供する。骨格としての機能だけでなく刺激に応答して細胞膜脂質から多種類の脂質性シグナル分子が産生される。また生体のエネルギー源、生理活性物質として正常な生体の働きを支える重要な化合物でもある。リピドミクスで扱う脂質は多様であるが、化学構造に基づき図５A のように簡便に整理しておくと代謝経路との関係が明瞭になり理解しやすい。すなわち、アセチルコエンザイム A(CoA)から生合成され炭素、水素、酸素のみからなる単純脂質とリン、窒素、硫黄なども含みグリセロールあるいはスフィンゴシンを骨格とする複合脂質に大別できる。単純脂質は複合脂質の構成成分でもある。

三大栄養素のうち糖とアミノ酸代謝は関連が深く、原則として解糖系とクエン酸回路の３から５個の炭素からなる代謝中間体を介して複雑に連携する。一方、脂質代謝は比較的閉じた代謝系を形成する。脂質のデノボ合成系の概略(図６)に示すように糖・アミノ酸代謝と脂質代謝間の架け橋は３本である。この橋を通してアセチル CoA からアシル CoA とステロイドが合成され、解糖系中間体ジヒドロキシアセトンリン酸からグリセロール骨格が 3-ホスホグリセリン酸から合成されるセリンとアシル CoA か

らスフィンゴシン骨格が合成される。これらをもとに図５Ａにまとめた全ての脂質がグルコースから生合成される(図６)。なお脂質に付加する糖はグルコース-6 リン酸から供給される。次に脂質分解系を考えてみる。複合脂質から加水分解酵素作用で遊離した脂肪酸はβ酸化され生成したアセチル CoA は直接あるいはケトン体として輸送された後に完全酸化され二酸化炭素になるので糖代謝系に戻れない。上述した脂質骨格もリサイクル利用可能である。以上のように、脂質代謝系内の代謝中間体が他の代謝系と頻繁に交換することがないという意味の閉鎖性により、リピドミクスから得られた脂質組成異常情報から関連蛋白質を推測しやすくプロテオミクス解析の効率化を助けることができる。

脂質分解系のもう一つの重要な機能は、多彩な脂質性シグナル分子や生理活性脂質を産生することである。小胞体シトゾール側でデノボ合成されたリン脂質中の特に *sn*-2 位脂肪酸は、多くの場合リモデリング酵素系によりすげ替えられ鎖長・不飽和度が変更され、目的の細胞内小器官膜に輸送される。これらの膜脂質から刺激に応答したホスホリパーゼ等の酵素作用で脂質性シグナル分子が合成される。これらにはリン酸化、酸化、過酸化などにより，もはや脂質と呼べない極性の化合物も含まれるが、リピドミクスの重要な標的である。

リピドミクスのデータ解析や多施設間データ比較のため脂質のデータベース化が必要である。最近、このような目的のために国際会議により吟味された包括的な分類が提案された(図５Ｂ)[1]。脂質は 12 桁の LIPID ID により識別される。初めの 2 桁はデータベース名、次の 2 桁には 8 種類のカテゴリーコード、さらに細目として各カテゴリーに属する脂質のうち化学構造に共通の骨格を持つ一群の脂質である脂質クラス 2 桁・サブクラス 2 桁・サブクラスに属する個々の脂質（分子種）の 4 桁識別番号からなる。これは米国 LIPID MAPS (http://www.lipidmaps.org/)により公開・維持されており、2006 年 9 月現在で 8906 件の登録がある。日本オリジナルの Lipid Bank (http://lipidbank.jp/; LIPID ID のデータベース名、LB)も公開され利用されている。

(2) リピドミクスにおける質量分析の利用法と問題点

脂質のイオン化法

脂質分析には、エレクトロスプレイ(ESI)、大気圧化学イオン化(APCI)、マトリクス支援レーザー脱離イオン化(MALDI)法などいわゆる“ソフト”イオン化法を用いることができるが、リピドミクスにはもっぱら高感度検出できる ESI が使われる。ESI に必要なエネルギーは“ソフト”イオン化法のうちで最も低く、一般にある程度電気伝導

性のある溶液に溶解しているイオン性あるいは極性化合物を対象とする。ESI は、エミッター(ESI チップ)内を流れる溶液と質量分析部の入り口の対極との間に高電圧を印加することによりエミッター出口に形成される液滴表面に電荷の分離が起こることから始まるので、そのイオン化効率は、この液滴表面の脂質の密度に依存する。ほとんどの脂質は多かれ少なかれ両親媒性で表面活性な性質を持つので液滴表面の脂質密度が大きくなり ESI で効率よくイオン化することができる。ESI は、HPLC やキャピラリー電気泳動とのオンライン接続に適しており、かつ APCI と異なり低流速でのイオン化に対応しているので細径カラムを用いることや、ナノスプレーチップ、チップ先端を超撥水性処理した FortisTip を用いることで高感度化できる。

イソプレノイド（例、スクワレンやコレステロール）などの一部の非極性脂質は、ESI によるイオン化効率が低いのでイオン性官能基の誘導体化等で ESI のイオン化効率を上げる工夫が必要である。また、APCI も用いられるが感度が不十分なことも多い。最近、このような脂質のイオン化に電子獲得 APCI がきわめて有効なことが明らかにされた。APCI イオン源においてコロナ放電により生じた高エネルギー電子が噴霧用窒素ガスと反応して N_2^+ラジカルと低エネルギー電子が生成される。電子親和性官能基を持つ化合物はこの低エネルギー電子を受け取り高効率に負イオン化される。これを利用すると、ESI や APCI でイオン化効率の悪い非極性脂質を電子親和性官能基で誘導体化することにより負イオンモードで 1-2 桁程度高い感度で検出が可能となる。

MALDI 法はマトリックス由来ピークの妨害を受けやすく、高速液体クロマトグラフィー（HPLC）とのオンライン接続も難しい。しかし糖脂質のように高分子量の脂質は、マトリックスによる妨害がないので薄層クロマトグラフィー(TLC)との組み合わせで MALDI-TOFMS がよく用いられている。脂質分析には通常 2,5-ジヒドロキシ安息香酸がマトリクスとして用いられるが、正イオンモードでは$[M+H]^+$以外に Na^+や K^+付加イオンなどに由来する複数のピークが混在した複雑なスペクトルとなり感度も低下するし、負イオンモードも低感度で実用的でない。最近、ニトロアニリンと酪酸のイオン性結晶をマトリックスとするとスペクトルが単純化され感度が上昇することが報告された。また、スフィンゴシン-1-リン酸やリゾホスファチジン酸を亜鉛含有リン酸捕獲試薬 Phos-tag で錯体として高分子量側にシフトさせ単一ピークとして検出する方法が試みられている。また、大気圧下でイオン化する AP-MALDI 法が開発され TOFMS 以外の質量分析計に接続しやすくなり、MALDI イオン源でもタンデム質量分析(MS/MS)が行いやすくなってきた。

脂質クラス分離と分子種分析

リピドミクスの目的からすれば、全脂質の包括的分析を一度にできれば理想的である。しかし、脂質は水にまったく溶けない非極性ものから、ミセルとして完全に溶解するものまで高範囲な極性のスペクトルを示すため（図７）、全ての脂質を一度に抽出する方法は現在のところ存在しない。定法の Folch 法や Bligh-Dyer 法で抽出した脂質には、非極性脂質とリン脂質が主に含まれるが、高極性の脂質の回収率は悪い。高極性脂質クラスはその物性にしたがった適当な方法で再抽出することが必要である。本稿では Folch 法などで抽出した脂質各クラスの分子種（構成脂肪酸の鎖長・二重結合数）組成を効率よく比較する方法について述べる。なお、中性ステロイドなど ESI でイオン化しにくい脂質クラスについては、前項で述べたイオン化法を用いた方法が開発されている[2)]。脂肪酸分析には多種類の構造異性体の二重結合数と位置決定が要求されるが、従来 GC/MS が、最近では二次元 GC×GC/MS による分析法が確立している。二重結合位置の決定には、局在化した正電荷を持つ官能基をカルボキシル末端に導入した際におこるチャージリモートフラグメンテーションを応用する。

粗抽出脂質をまずそのまま分析するが、相対的に微量成分のスフィンゴ脂質のみを対象とするときは、弱アルカリ(0.5-1 M NaOH)でグリセロ脂質中のエステルを加水分解した後に再抽出して分析する。この方が、多量に存在するトリアシルグリセロール（TG）やホスファチジルコリン(PC)を除去できるので感度の向上を期待できる。ただし、アセチル化などスフィンゴ脂質に存在するエステル結合も加水分解されるので注意が必要である。複雑な組成の粗抽出脂質に含まれる各種の脂質を分析する際に、まず脂質クラスの分離を行い、そのクラス内の分子種（脂肪酸組成）を分析するのが適当である。分子種分析はおもに MS の仕事であるが、クラス分離には質量分析器自身の分離機能を用いる方法[3)]と HPLC とのオンライン接続を用いる方法[4,5)]とがある。

質量分析器によるクラス分離では、極性頭基から由来するクラス特異的なフラグメントを用いたプリカーサイオンスキャンやニュートラルロススキャンを駆使してプロトン付加あるいはカチオン付加分子を系統的に検出する(表１)。さらに特定の脂肪酸に注目した脂肪酸アニオンに対するプリカーサイオンスキャンや正イオンモードでの脂肪酸あるいは[脂肪酸-H_2O](ケテン)のニュートラルロススキャンの結果も考慮して同定の精度を上げる。このような MS による分離機能と LiOH の添加による特定の脂質のシグナル増強効果を併用したリピドミクス分析が行われている[3)]。脂質をクロロホルム/メタノール(1:2 v/v)に溶解してまず負イオン ESI-MS 測定して酸性リン脂質（ホスファチジルセリン(PS)，ホスファチジルイノシトール(PI)，ホスファチジルグリセロ

ール(PG),カルジオリピン、スルファチド) の分子種解析をする。次に、LiOH メタノール溶液を加えて弱アルカリにすると PE とセラミドの負イオンシグナルが増強される。正イオンモードでは PC,スフィンゴミエリン(SM),TG、ガラクトシルセラミド等の Li^+ イオン付加体が形成され MS/MS による分子種情報取得が容易になる。

TLC 同様に(誘導体化)シリカゲルを用いる順相 HPLC では、原則として図7の非極性脂質から順に極性にしたがい溶出されるので主要な脂質分子を個々のクラスごとに分離することができる。逆相 HPLC では、主に脂質分子中炭化水素鎖の鎖長と不飽和度に依存する疎水性度に従って分離されるので、脂質の分子種分離に利用できる。同じ *m/z* 値の構造異性体を分離できる場合があるので、順相 HPLC で分離したフラクションを逆相 HPLC でさらに分離したり、MS によるクラス分離と併用したりすると分子種分析の精密化が期待できる[6]。なお、順相 HPLC においても、同じクラスに属する脂質が完全に同じ時間に溶出されるわけではなく、鎖長の長いものほど、二重結合が少ないものほど先に溶出される傾向がある。

中性脂質,リン脂質を一回の HPLC で分離するためには、ヘキサンなどの無極性溶媒(A) から水を含有する極性溶媒(C)への濃度勾配溶出が必要である。A と C 溶媒はお互いに混ざらないので中継ぎに両溶媒と混ざり合う溶媒 B が必要であり、3 溶媒濃度勾配溶出が必要になる。MS と接続するためには、HPLC の分離能以外にイオン化効率を保つ工夫も必要である。電気伝導性のないヘキサン主体の A 溶媒で先に溶出してくる中性脂質は ESI ができない。このため中性脂質が溶出してくる保持時間帯にギ酸アンモニウムを含むイオン化促進用極性溶媒を溶出液とティーを介して混合すると、コレステロールエステル(CE)、ワックス、TG 等の非極性中性脂質も NH_4 付加正イオンとして効率良くイオン化される。無極性溶媒を用いる HPLC は、脂肪酸酸化誘導体やエイコサノイドのキラール分離にも用いられる。この場合には対象脂質を電子親和性ペンタフルオロベンジル化した後にキラール HPLC/電子捕獲 APCI/MS(MRM モード)で高感度一斉分析するキラールリピドミクスシステムが開発されている[7]。

順相 HPLC にオンライン接続する質量分析計には、HPLC との接続性が良く高感度に MS スペクトルと全溶出範囲のプロダクトイオンスペクトルを自動的に測定できるイオントラップ質量分析計あるいはリニアイオントラップ質量分析計を使用するのが便利である。ある保持時間にカラムから溶出してきた脂質分子種混合物の MS スペクトルから、あらかじめ設定した閾値よりシグナル強度が大きいイオンを抽出し、強度の強いピークから順に複数の分子種のプロダクトイオンスペクトルを測定するイオントラップ型装置の機能により分子種組成分析を効率化できる。この機能をデータ依存的

(data-dependent)MS/MS スキャンということがあり、学術用語ではないが簡潔に機能を表す便利な用語であるので英文ジャーナルではよく用いられ本節でも用いる。なお、目的によりプロダクトイオンスペクトルは MS/MS スペクトルだけではなく、MS/MS で生成した一つのフラグメントイオンをさらに開裂させスペクトルを得る機能をもちいることも可能である。このように複数回開裂を繰り返し構造情報を得やすくする方法を、MS^n スキャンと呼ぶことがありこれも便利であるので英文ジャーナルでは良く用いられおり本節でも使用する。ここで上付き添え字 n は、開裂回数＋1 を意味する。ThermoFisherSientific 社の LCQ イオントラップ型装置では、交互に正負極性を切り替えながらどちらかの極性のデータ依存的 MS^n スキャンを行うことが可能で一回のクロマトグラフィーで多くの情報を採取することができる。スクリーニング分析では、前半の中性脂質が溶出する時間帯には正イオン MS/MS スキャンを行い、後半のリン脂質溶出時間帯には負イオン MS/MS スキャンをすれば分子種情報を得やすい。PC の正確な分子種同定には MS/MS スキャンで生じた$(M-H+HCOO-60)^-$イオンをもう一度開裂させるデータ依存的 MS^3 スキャンが有用である。図８A はこのようにして得た、指定した m/z 範囲内で、各保持時間における最強シグナル強度をプロットしたクロマトグラム（ベースピーククロマトグラム）（m/z = 400-1600）である。脂質クラス構成の全貌を鳥瞰できるので、新規の脂質の発見や脂質代謝異常の同定も容易になる。各脂質クラスのに特徴がありクラスの同定や混在ピークの検出に有用である(表２)。図８B-C には脂質クラスの MS スペクトルと同定した分子種組成の例を示す。

三連四重極質量分析計の検出器側の四重極にリニアイオントラップの機能を持たせた Applied Biosystems 社 4000Q トラップ装置では、プリカーサイオンスキャンやニュートラルロススキャン機能も利用することができる。リン脂質分子種を逆相 HPLC で分離してオンラインでこれらの MS/MS モードを行いクラス分離と分子種分離同定を精密化する試みも行われている。また、MRM モードを用いて微量成分である酸化リン脂質などの高感度同定も試みられている。順相 HPLC を用いる時、図８のようなクロマトグラムから得られる保持時間とイオンの m/z 値から脂質クラスを容易に帰属することができる(さらに MS^n スペクトルで確認できる)。逆相 HPLC 分離では保持時間をクラス同定に使えないので、MS/MS モードによって脂質クラスを同定しなければならない。なお、MS スペクトルの生データから脂質を同定する解析ソフトウエア Lipid Search (http://lipidsearch.jp/LipidNavigator.htm) が公開されており利用することができる。

リピドミクスにおいて膨大な数の脂質分子種の個々について薬物動態分析のように

同位体希釈法を用いて正確な定量をするのは不可能である。次善の策として各脂質クラスにつき内因性シグナルがほとんどない分子種（通常は短鎖の脂肪酸を含有する分子種）を一つ内部標準として加え半定量する。この際、内部標準物質(IS)の炭素数(s)と定量すべき脂質分子種の炭素数(n)が異なるので天然に1%の割合で混在する ^{13}C 同位体の影響を補正しなければならない。すなわち、炭素数が増えるほど、^{13}C を1つ含むイオン M+1 や2つ含むイオンM+2のピーク強度が相対的に大きくなるので ^{13}C を含まないモノアイソトープイオンMのピークの強度(I_M)が減少する。実測した I_M/I_M^{IS} と定量計算に必要な同位体ピークを足し合わせた全強度(I_{total})の比(I_{total}/I_{total}^{IS})には ^{13}C を三個以上含むイオンのピーク強度は小さいので無視すると、以下の関係がある。$n \neq s$ なら右辺係数で実測値を補正する。

$$\frac{I_{total}}{I_{total}^{IS}} = \frac{I_M}{I_M^{IS}} \frac{\left[1 + 0.011n + 0.011^2 \frac{n(n-1)}{2}\right]}{\left[1 + 0.011s + 0.011^2 \frac{s(s-1)}{2}\right]}$$

また、脂肪酸の二重結合数が異なる分子種が混在する時は、定量したい M イオンより二重結合が 1 つ多いため 2 u 小さい分子種イオンの M+2 ピークの重なりも $(0.011)^2 n(n-1) I_{M-2}/2$ をさし引いて補正する。HPLC を用いる方法では、ピーク強度ではなく各分子種のイオンクロマトグラムのピーク面積を用いてこれらの補正をする。脂肪酸の長さによるイオン化効率の違いの補正も必要な場合には実験で補正係数を決めて適用する必要がある。幸い、リン脂質やセラミドでは、イオン化効率はそれほど鎖長に依存しない。

リピドミクス解析のうち順相 HPLC を用いる方法は、遺伝子操作マウスの脂質異常や臨床サンプルの測定に応用され、その実用性と有効性が確かめられた 4, 5)。MS の分離機能を用いる方法も臨床サンプル測定や植物への寒冷ストレスの影響の検討で有効性と実用性が確かめられている 3)。今後さらに測定できる脂質クラスレパートリーを増やして、真に包括的で大規模な臨床リピドミクス解析などに耐えるシステムに成長していくことが望まれる。

文献

1. E. Fahy, S. Subramaniam , HA. Brown, CK. Glass, AH Jr Merrill, RC. Murphy, CR. Raetz, DW. Russell, Y. Seyama, W. Shaw, T. Shimizu, F. Spener, G. van Meer, MS. VanNieuwenhze, SH.White, JL.Witztum, and EA. Dennis, *J Lipid Res.* **6**, 839-861 (2005)
2. Y, Wang, K. Karu, and WJ. Griffiths, *Biochimie*, in press (web version available) (2006)
3. X. Han and RW. Gross, *Mass Spectrom. Rev.* **24**, 367-412 (2005)
4. 東城博雅　オレオサイエンス **4**, 3-12 (2004)　Y. Nagatsuka, H. Tojo. Y. Hirabayahsi, *Methods Enzymol.* 417, 155-167 (2006)
6. T. Houjyou, K. Yamatani, M. Imagawa, T. Shimizu, and R. Taguchi, *Rapid Commun. Mass Spectrom.* **19**, 654-666 (2005)
7. SH. Lee, MV. Williams. and IA. Blair, *Prostaglandins Other Lipid Mediators* **77**, 141-157 (2005)

図の説明

図５ 脂質の分類

B, データベースには現在 LM の他に、LB, Lipid Bank (http://lipidbank.jp); LD, LIPIDAT (http://www.lipidat.chemistry.ohiostate.edu)がある。

図６．脂質代謝の特徴

TCA、クエン酸回路 –P、リン酸

図７．脂質分子極性のスペクトルと順相 HPLC 溶媒の選択

点線より右側の高極性脂質の抽出時、蛋白質や非脂質の不純物が混入しやすく分析を妨げられることが多いので、それらの物性に従い最適な抽出法を選択しなければならない。

図８．ケラチノサイトから抽出した脂質の順相 HPLC/MS による分析例。

略号は表 2 と同じ。A,' 正負の極性を交互切替かえながら取得した正負ベースピーククロマトグラム（m/z＝400-1600)。B, ラベルした脂質の正イオンマススペクトル。C, ラベルした脂質の負イオンスペクトル。数字はそれぞれのピークの *m/z* 値、コロンで区切った数字は脂肪酸の炭素数：二重結合数を示す。二段の数字の上段は sn-1 位の脂肪酸組成で p はプラスメニル基（ビニルエーテル結合）を示す。下段は sn-2 位の脂肪酸。sn-2 位の脂肪酸の方が開裂しやすいので MS/MS スペクトルの脂肪酸のニュートラルロスピークが大きい。

表１．脂質クラス同定に有用なMS/MSモードとフラグメント

脂質クラス	前駆イオン	MS^2モード	*m/z*	Fragments
	負イオン			
グリセロリン脂質	$[M-H]^-$	PR	153	Glycerol-3-phosphate – H_2O
PC	$[M+Cl]^-$	NL	50	Methylchloride
PC, SM	$[M+HCOO]^-$	NL	60	CH_3+HCOO
PE	$[M-H]^-$	PR	196	Glycerol-P-ethanolamine – H_2O
PS	$[M-H]^-$	NL	87	Serine – H_2O
PI	$[M-H]^-$	PR	241	Phosphoinositol – H_2O
Ceramide	$[M-H]^-$	NL	240	2-Hexadecenol
sulfatide	$[M-H]^-$	PR	97	Sulfate
	正イオン			
PC, SM	$[M+H]^+$	PR	184	Phosphoholine
	$[M+Li]^+$	NL	59	Trimethyamine
	$[M+Li]^+$	NL	183	Phosphoholine
PE	$[M+H]^+$	NL	141	Phosphoethanolamine
PS	$[M+H]^+$	NL	185	Phosphoserine
PI	$[M+NH_4]^+$	NL	277	Phosphoinositol+NH_4
PG	$[M+NH_4]^+$	NL	189	Phosphoglycerol+NH_4

略号は、表２を参照。PR, プリカーサイオンスキャン；　NL,ニュートラルロススキャン